Strong *K*-edge Magnetic Circular Dichroism Observed in Photon-in–Photon-out Spectroscopy

Marcin Sikora,[1,*] Amélie Juhin,[2,†] Tsu-Chien Weng,[3] Philippe Sainctavit,[4] Carsten Detlefs,[3]
Frank de Groot,[2] and Pieter Glatzel[3,‡]

[1]*Faculty of Physics and Applied Computer Science, AGH University of Science and Technology, 30-059 Kraków, Poland*
[2]*Department of Inorganic Chemistry and Catalysis, Utrecht University, 3584 CA Utrecht, The Netherlands*
[3]*European Synchrotron Radiation Facility, BP 220, 38043 Grenoble Cedex, France*
[4]*Institut de Minéralogie et de Physique des Milieux Condensés (IMPMC), UMR CNRS 7590, Université Pierre et Marie Curie, IPGP,
75052 Paris Cedex 05, France*

A large enhancement of the x-ray magnetic circular dichroism is observed at the iron *K* absorption preedge of magnetite. This is achieved by performing resonant inelastic x-ray scattering (RIXS) experiments with a $2p$ hole in the final state of the second-order optical process. We measured and calculated the full $1s2p$ RIXS planes for opposite helicities of the incoming circularly polarized x rays. The crystal field multiplet calculations show that the enhancement arises from $2p$-$3d$ Coulomb repulsions and $2p$ and $3d$ spin-orbit coupling. The observed magnitude of the RIXS magnetic circular dichroism effect is ~16%. This opens up new opportunities for a broad range of research fields allowing for truly bulk-sensitive, element-, and site-selective measurements of $3d$ transition metal magnetic moments and their ordering using hard x-ray photons.

X-ray magnetic circular dichroism (XMCD) is a powerful tool for the element-specific study of the magnetic structure of complex systems [1–3]. It enables at spin-orbit split absorption edges to determine spin and orbital magnetic moments by means of sum rules [4,5]. It has been almost 25 years since the effect of magnetic dichroism was anticipated for the x-ray absorption spectra [6] and the first experimental observations of the linear [7] and circular [8] x-ray magnetic dichroism spectra were reported. Over the years the techniques became a routine probe of element-specific magnetization in antiferro- and ferro(ferri)-magnetic systems [9,10].

The magnetic moments of $3d$ transition metals (TM) are generally studied at the L absorption edge, i.e., dipole-allowed $2p \rightarrow 3d$ transitions using soft x rays. Soft x-ray XMCD measurements are typically performed using total electron yield, because significant self-absorption effects that distort the spectral shape are observed when using total fluorescence yield detection. Thus, *L*-edge XMCD is mainly sensitive to the sample surface and, in addition, it is not compatible with demanding sample environments such as high-pressure cells, due to short penetration depth. Therefore, the $3d$ TM element-specific studies of bulk magnetic properties under extreme conditions, that require the penetrating properties of hard x rays, have been using *K*-edge XMCD [11,12] and $K\beta$ emission spectroscopy [12–15]. The latter is sensitive only to the spin and orbital momenta (S and L) of individual ions, but not to the magnetic moments (m_s and m_l). As such, it does not provide quantitative information on interatomic magnetic interactions. The magnetic signal in *K*-edge XMCD is very weak and the absence of spin-orbit split edges prohibits a

detailed quantitative interpretation. There is hence a need for a magnetic spectroscopy in the hard x-ray range that can provide information on the ordering and the value of magnetic moments. We show in this Letter that this goal can be achieved by combining XMCD with $1s2p$ resonant inelastic x-ray scattering (RIXS) at the *K* absorption preedge.

A RIXS signal was observed for the first time in the early 1970s [16], but the technique only developed its full potential with the advent of x-ray synchrotron radiation sources. With improved instrumentation [17] and a deeper theoretical understanding [18] this photon-in–photon-out spectroscopy has turned into an important analytical tool to study the electronic structure of TM compounds [19]. RIXS is a second-order optical process where the deep core hole in the intermediate state is replaced by a shallower hole in the final state. This results in sharp spectral features and often a rich multiplet structure that reveals electron-electron and spin-orbit interactions. Magnetic dichroism measurements have been combined with RIXS previously, but these studies were mainly performed at the $L_{2,3}$ absorption edges, probing low energy transfer excitations in $3d$ TM [20,21] or the quadrupole transitions ($2p \rightarrow 4f$) in lanthanides [22–26].

The $1s2p$ RIXS probes the evolution of $K\alpha$ emission ($2p \rightarrow 1s$) following resonant excitation of a $1s$ electron. The *K*-edge absorption spectra of most $3d$ TM compounds show weak preedge features that arise from quadrupole ($1s \rightarrow 3d$) excitations and possibly additional dipole ($1s \rightarrow 4p$) transitions. The intensity of the latter depends on the degree of $3d$-$4p$ orbital hybridization and thus the local symmetry around the TM ion [27]. The *K* preedge is

sensitive to the valence orbitals that are predominantly composed of the $3d$ density of unoccupied states. The $2p^5 3d^{n+1}$ final state electron configuration in $1s2p$ RIXS is identical to the $2p$ spin-orbit split $L_{2,3}$ absorption edges [28]. The idea of the present work is to combine $1s2p$ RIXS in $3d$ transition metals with XMCD.

The measurements were performed at beam line ID26 of the European Synchrotron Radiation Facility using incoming radiation from the undulator fundamental. The incident energy was selected by means of a pair of Si(311) crystals. The circular polarization of the incident x rays was achieved using a 500 μm thick diamond (111) quarter wave plate (QWP). The inelastically scattered photons were analyzed using a set of four spherically bent Ge(440) crystals that were arranged with sample and photon detector (Avalanche Photo Diode) in a vertical Rowland geometry ($R \approx 1$ m). The scattering angle was set to 90° with sample surface at 45° to the incident beam. The combined resolution of the setup was determined using the full width at half maximum of the elastically scattered peak to $\Delta E = 1.4(1)$ eV. The $1s2p$ RIXS-MCD spectrum was acquired at room temperature from a polycrystalline sample of magnetite $[Fe^{III}]_{tetra}[Fe^{II}Fe^{III}]_{octa}O_4$ as a set of constant emission energy scans over the energies of the $K\alpha_1$ and $K\alpha_2$ fluorescence lines. The sample was kept in magnetic saturation with the magnetization vector parallel to the incident beam using a $Nd_2Fe_{14}B$ permanent magnet, while the photon helicity was reversed after every two constant emission energy spectra. The constant degree of circular polarization, $P_C \sim 75(5)\%$, was maintained by

simultaneous scanning of the incident photon energy and θ_{QWP}. The spectra are normalized to perfect circular polarization degree (i.e., divided by P_C), but they are not corrected for self-absorption effects. The latter may considerably affect the shape and dichroism of the main K edge. In the preedge range, however, they are weak and do not influence the analysis presented here.

Figure 1 presents the RIXS planes, i.e., the observed fluorescence intensity as a function of energy transfer and incident photon energy. The energy transfer is the difference between incident and emitted energy. The RIXS signal shown in Fig. 1 is averaged over both photon helicities, whereas the RIXS-MCD signal [Fig. 1(b)] is obtained by taking their difference. Their comparison shows that only the resonant features give rise to the XMCD, while the features due to nonresonant fluorescence, that are visible as diagonal structures in the RIXS plane, do not show any detectable XMCD effect. The experimental RIXS-MCD plane reveals two groups of final states, which correspond, respectively, to the $K\alpha_1$ and $K\alpha_2$ emission lines. They are each composed of two strong features with different spin polarization, and the sign of their XMCD is opposite. The characteristic dispersion of the resonant features is due to the lifetime of the $1s$ hole along the incident energy and of the $2p$ hole along the energy transfer. The experimental data are compared with the theoretical spectrum calculated within the crystal field multiplet approach [Fig. 1(c) and 1(d)].

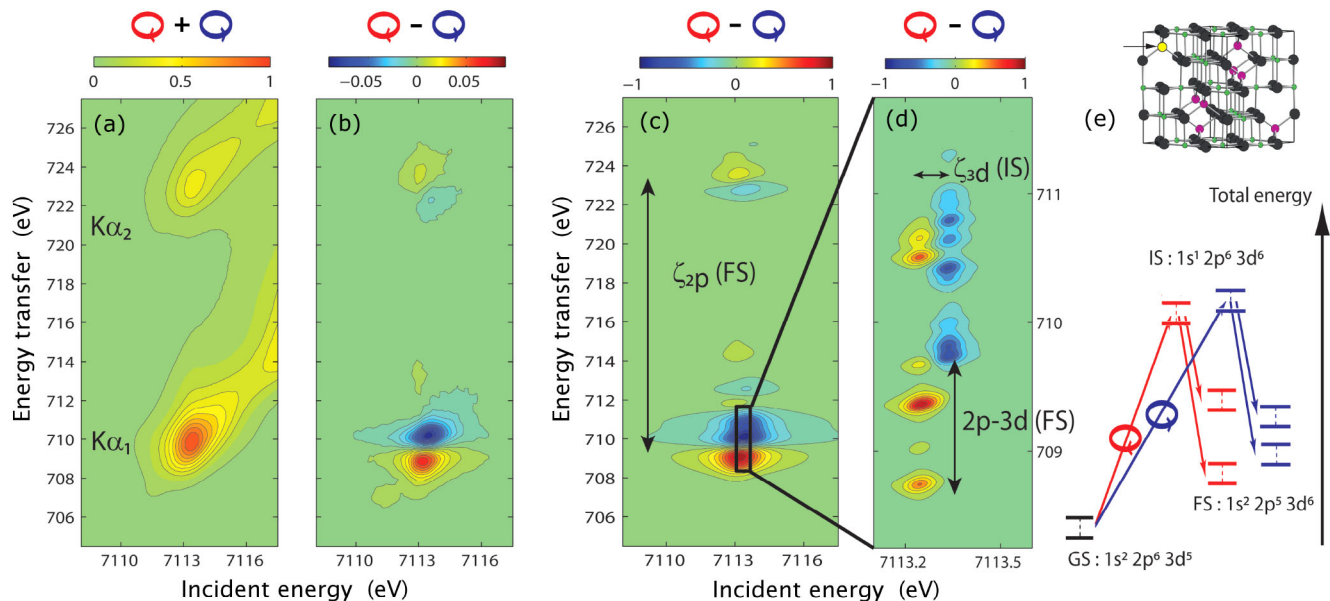In a first step towards a quantitative simulation of the $1s2p$ RIXS-MCD signal, we considered only the contri-

FIG. 1 (color online).   (a) The $1s2p$ RIXS plane measured at the Fe K edge in magnetite. (b) The RIXS-MCD plane, plotted as the difference between the RIXS planes measured for opposite helicities of circularly polarized light. (c) The theoretical RIXS-MCD plane calculated for tetrahedral Fe^{III}. (d) The theoretical RIXS-MCD plotted for the $2p_{3/2}^5 3d^6$ final state with a small broadening reveals the origin of the energy shifts that give rise to the dichroism. The arrows with labels indicate the interactions to which the splittings are proportional. (e) Energy level diagram that was used in the crystal field multiplet calculations, involving only a tetrahedral Fe^{III} ion of magnetite [arrow marked (yellow) atom in structure]. See text for details.

bution from tetrahedral Fe^{III}. The lack of inversion symmetry enables $3d$-$4p$ hybridization resulting in strong $1s \rightarrow 4p$ dipole contributions to the preedge, while only weak $1s \rightarrow 3d$ quadrupole transitions are present for the octahedral Fe sites [19]. The spectrum was simulated using the crystal field multiplet approach developed by Thole *et al.* [29]. We considered an electric quadrupole excitation from $1s^2 2p^6 3d^5$ (ground state, GS) to $1s^1 2p^6 3d^6$ (intermediate state, IS), followed by an electric dipole emission to $1s^2 2p^5 3d^6$ (final state, FS), as shown schematically in Fig. 1(e) [30]. The radial integrals for interelectronic repulsion and spin-orbit coupling were calculated using the atomic Hartree-Fock code of Cowan [31], where the Slater integrals were scaled down to 80% in agreement with previously published experimental works. The effects of the crystal field and of the magnetic exchange field were considered using the $O_3 - T_d - S_4$ branching [32]. Values of $10Dq = 0.6$ eV and $g\mu_B B = -10$ meV were taken for the crystal field and the exchange field, respectively. The RIXS cross section was calculated using the Kramers-Heisenberg formula for a right-circular and a left-circular polarization vector. The transition lines were convoluted using a Lorentzian and a Gaussian function to account for the core-hole lifetime and instrumental resolution, respectively. For the Lorentzian, the half width at half maximum was chosen as 0.75 eV (IS) and 0.15 eV (FS). The half width of the Gaussian is 0.25 eV.

The experimental and theoretical RIXS-MCD planes [Figs. 1(b) and 1(c)] are in good agreement, in particular, with respect to the energy splittings and relative transition strengths of the left and right polarized channels. The theoretical plane shows additional features along the energy transfer direction, in particular, at higher energies of the $2(p_{3/2})^5 3d^{n+1}$ ($K\alpha_1$) final states. These discrepancies are likely smoothed in experiment due to convolution with the energy-dependent lifetime broadening and experimental resolution function. The experimental data show a weak feature at 7112 eV incident energy and 707 eV energy transfer that is not observed in the calculations. This feature can be ascribed to octahedral Fe^{II}, considering that (i) its K preedge [27] and L edges [33] are shifted by -1.5 eV with respect to Fe^{III}, and (ii) this feature is absent from the RIXS-MCD measured on a $Mn[Fe^{III}]_2 O_4$ (not shown). The low intensity of the Fe^{II}-induced XMCD signal and the good agreement between the experimental and calculated RIXS-MCD planes justify *a posteriori* the assumptions made in the calculation.

The overall agreement of the experimental results with a simple ionic crystal field model provides the possibility for a fundamental understanding of the RIXS-MCD effect. We show the theoretical RIXS-MCD plane at the $K\alpha_1$ resonance in Fig. 1(d). The line broadenings were reduced in order to reveal the underlying interactions. The states that give rise to the XMCD in the $1s^1 3d^6$ intermediate state are split by the $3d$ spin-orbit coupling and the exchange field. They are reached by left and right circular polarized x rays

with 100% selectivity and decay into final states with different orbital and spin momenta that are split by $2p$-$3d$ Coulomb repulsion. In the RIXS-MCD plane, the energy shift between left and right polarization along incident energy and energy transfer is thus mainly given by the $3d$ spin-orbit coupling in the intermediate state and the $2p$-$3d$ Coulomb repulsions combined with the $2p$ spin-orbit interaction in the final state, respectively. As a consequence, one can expect strong XMCD enhancement in RIXS spectra of those systems that reveal well-defined preedge features as it is the case in, e.g., semiconductors and molecular complexes. Itinerant and metallic systems generally do not show distinct spectral features that can be assigned to dominantly $3d$ orbitals possibly limiting the enhancement of the XMCD effect. However, this preliminary assertion has to be tested in future experiments.

A striking consequence of combining RIXS with XMCD is a dramatic enhancement of the dichroism as compared to conventional K-edge absorption measurements. Figure 2(a) compares the Fe K-edge spectra of magnetite measured at the maximum of the $K\alpha_1$ emission to the $K\alpha_{1,2}$-integrated spectra, i.e., the RIXS spectral intensity summed over the energy transfer. The latter is equivalent to conventional fluorescence-detected absorption spectroscopy, while the $K\alpha_1$-detected spectrum corresponds to a diagonal cut through the RIXS plane. Both spectra reveal similar features with a broad preedge peak at $\sim$7113.5 eV. The $K\alpha_1$-detected spectrum shows sharper spectral features due to the reduced lifetime broadening [34,35]. The $K\alpha_{1,2}$-integrated XMCD spectrum [Fig. 2(b)] shows a shape that is similar to what was observed in previous
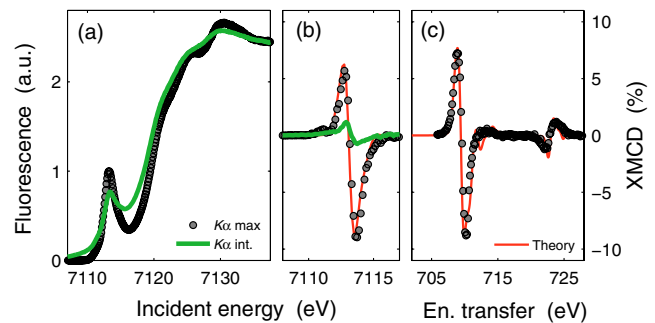

FIG. 2 (color online). Line scans extracted from the RIXS-MCD plane. Comparison of the Fe K edge spectra (a) and their magnetic circular dichroism (b) acquired at the maximum of $K\alpha_1$ fluorescence line (dots) and using the $K\alpha_{1,2}$-integrated spectrum [thick (green) line]. The $K\alpha_1$-detected XMCD spectrum shows almost eightfold enhancement of the dichroism as compared to $K\alpha_{1,2}$-integrated and is in good agreement with the theoretical spectrum [thin (red) line]. (c) Comparison between theoretical [thin (red) line] and experimental (dots) XMCD spectra acquired at constant incident photon energy, which corresponds to a vertical line through the RIXS-MCD plane at the incident energy of 7113.6 eV. The measured XMCD effect shown in (b) and (c) is relative to the maximum preedge intensity, while the intensity of the theoretical XMCD is scaled down by factor of 5.67 to obtain best match.

experiments [36] and band structure calculations [37]. However, the intensity of the $K\alpha_1$ detected XMCD is strongly enhanced and shows a peak-to-peak amplitude as large as 16% of the preedge maximum [Fig. 2(b)]. The RIXS-MCD plotted as a function of the energy transfer at constant incident energy [Fig. 2(c)] corresponds in the final states to L-edge absorption spectroscopy. We observe the same order of magnitude in the XMCD signal as what has been reported at the Fe L_3 edge in magnetite [38,39]. The crystal field multiplet calculations show that the enhancement of the XMCD signal in RIXS is a result of reduced lifetime broadening and increased splitting of the XMCD spectral features in the $2p^5 3d^{n+1}$ final state.

An interesting aspect of RIXS-MCD is the possibility for site-selective measurements in mixed valence and multisite compounds. The incident and emission energies depend on the oxidation state of the absorber and it is possible to increase the selectivity by tuning either of these, for example, on the weak feature at 7012 eV incident and 707 eV transfer energy in Fig. 1(b), in order to study the magnetic behavior of octahedrally coordinated Fe^{II} in magnetite. Therefore, $1s2p$ RIXS-MCD can be adopted for element- and site-selective magnetometry and magnetic microscopy of $3d$ TM with hard x rays, by monitoring the changes in the XMCD amplitude as a function of space, pressure, temperature, or time, either in line scans or, if time allows, by measuring the full RIXS plane. Supported by crystal field multiplet calculations and using RIXS sum rules [40,41], this could be used to extract the values of many GS moments by using angle-dependent experiments. Although the applicability of sum rules has to be confirmed, the significant progress achieved in synchrotron radiation sources and beam lines equipped with high resolution fluorescence spectrometers will allow the technique to become widely accessible.

———————————

*marcin.sikora@agh.edu.pl
†A.F.Juhin@uu.nl
‡glatzel@esrf.fr

[1] H. A. Dürr et al., Science **277**, 213 (1997).
[2] P. Gambardella et al., Nature (London) **416**, 301 (2002).
[3] M. Mannini et al., Nature Mater. **8**, 194 (2009).
[4] B. T. Thole, P. Carra, F. Sette, and G. van der Laan, Phys. Rev. Lett. **68**, 1943 (1992).
[5] P. Carra, B. T. Thole, M. Altarelli, and X. Wang, Phys. Rev. Lett. **70**, 694 (1993).
[6] B. T. Thole, G. van der Laan, and G. A. Sawatzky, Phys. Rev. Lett. **55**, 2086 (1985).
[7] G. van der Laan et al., Phys. Rev. B **34**, 6529 (1986).
[8] G. Schütz et al., Phys. Rev. Lett. **58**, 737 (1987).
[9] C. T. Chen et al., Phys. Rev. B **48**, 642 (1993).
[10] J. Stöhr, J. Magn. Magn. Mater. **200**, 470 (1999).
[11] O. Mathon et al., Phys. Rev. Lett. **93**, 255503 (2004).
[12] Y. Ding et al., Phys. Rev. Lett. **100**, 045508 (2008).
[13] J. Badro et al., Science **300**, 789 (2003).
[14] J. Badro et al., Science **305**, 383 (2004).
[15] J.-F. Lin et al., Nat. Geosci. **1**, 688 (2008).
[16] C. J. Sparks, Phys. Rev. Lett. **33**, 262 (1974).
[17] K. Hämäläinen, D. P. Siddons, J. B. Hastings, and L. E. Berman, Phys. Rev. Lett. **67**, 2850 (1991).
[18] P. Carra, M. Fabrizio, and B. T. Thole, Phys. Rev. Lett. **74**, 3700 (1995).
[19] F. de Groot and A. Kotani, *Core Level Spectroscopy of Solids* (CRC Press, Boca Raton, 2008).
[20] L. Braicovich et al., Phys. Rev. Lett. **82**, 1566 (1999).
[21] L. Braicovich et al., Phys. Rev. Lett. **95**, 267402 (2005).
[22] T. Iwazumi et al., Phys. Rev. B **56**, R14267 (1997).
[23] F. M. F. de Groot, M. Nakazawa, A. Kotani, M. H. Krisch, and F. Sette, Phys. Rev. B **56**, 7285 (1997).
[24] F. M. F. de Groot, M. H. Krisch, F. Sette, and J. Vogel, Phys. Rev. B **62**, 379 (2000).
[25] K. Fukui, H. Ogasawara, I. Harada, and A. Kotani, J. Synchrotron Radiat. **8**, 407 (2001).
[26] T. Nakamura et al., J. Synchrotron Radiat. **8**, 428 (2001).
[27] T. E. Westre et al., J. Am. Chem. Soc. **119**, 6297 (1997).
[28] W. A. Caliebe et al., Phys. Rev. B **58**, 13452 (1998).
[29] B. T. Thole et al., Phys. Rev. B **32**, 5107 (1985).
[30] For the tetrahedral Fe^{III} site ($^6A_1$ ground state) the electric dipole ($E1$) operator has T_2 symmetry and the electric quadrupole ($E2$) operator has T_2 and E symmetries. In the present case, the quadrupole operators for left and right polarized light ($2\tilde{1}11$ and $2\tilde{1}1$–1) only select T_2 transitions and not E transitions. Then the only symmetry reached in the intermediate state is T_2 symmetry: T_2 (hybridized $4p$-$3d$) for $E1$ transitions and T_2 (pure $3d$) for $E2$ transitions. Since all the intermediates states have T_2 symmetry with a dominant $3d$ character, we restricted the calculation to $E2$ transitions in order to limit the number of free parameters.
[31] R. D. Cowan, *The Theory of Atomic Structure and Spectra* (University of California Press, Berkeley, 1981).
[32] P. H. Butler, *Point Symmetry Group Applications* (Plenum Press, New York, 1981).
[33] P. Kuiper, B. G. Searle, L.-C. Duda, R. M. Wolf, and P. J. van der Zaag, J. Electron Spectrosc. Relat. Phenom. **86**, 107 (1997).
[34] K. Hämäläinen et al., Phys. Rev. B **46**, 14274 (1992).
[35] P. Glatzel and U. Bergmann, Coord. Chem. Rev. **249**, 65 (2005).
[36] K. Matsumoto et al., Jpn. J. Appl. Phys. **39**, 6089 (2000).
[37] V. N. Antonov, B. N. Harmon, and A. N. Yaresko, Phys. Rev. B **67**, 024417 (2003).
[38] D. J. Huang et al., Phys. Rev. Lett. **93**, 077204 (2004).
[39] C. Carvallo et al., Am. Mineral. **93**, 880 (2008).
[40] M. van Veenendaal, P. Carra, and B. T. Thole, Phys. Rev. B **54**, 16010 (1996).
[41] F. Borgatti et al., Phys. Rev. B **69**, 134420 (2004).